CELLULAR IMAGING OF THE TAPETAL-LIKE REFLEX IN CARRIERS OF *RPGR*-ASSOCIATED RETINOPATHY

ANGELOS KALITZEOS, PhD,*† RANJIT SAMRA, MBChB,*† MELISSA KASILIAN, BA,*†
JAMES J. L. TEE, FRCOphth,*† MARGARET STRAMPE, BA,‡§ CHRISTOPHER LANGLO, PhD,‡
ANDREW R. WEBSTER, FRCOphth,*† ALFREDO DUBRA, PhD,¶ JOSEPH CARROLL, PhD,‡**
MICHEL MICHAELIDES, FRCOphth*†

Purpose: To examine the features of the tapetal-like reflex (TLR) in female carriers of RPGR-associated retinopathy by means of adaptive optics scanning light ophthalmoscopy (AOSLO) and spectral domain optical coherence tomography.

Methods: Nine molecularly confirmed RPGR carriers and three healthy controls underwent ocular examination and the following retinal imaging modalities: color photography, near-infrared reflectance, fundus autofluorescence, spectral domain optical coherence tomography, and AOSLO. After identifying TLR areas across all imaging modalities, normalized local contrast of outer retinal bands on spectral domain optical coherence tomography was calculated and AOSLO-acquired photoreceptor mosaic analysis was performed.

Results: Seven carriers had TLR areas, which colocalized with increased rod photoreceptor reflectivity on confocal AOSLO and reduced cone photoreceptor densities. Parafoveal TLR areas also exhibited reduced local contrast (i.e., increased reflectivity) of the outer retinal bands on spectral domain optical coherence tomography (inner segment ellipsoid zone and outer segment interdigitation zone). Healthy controls did not show TLR.

Conclusion: The cellular resolution provided by AOSLO affords the characterization of the photoreceptor mosaic in RPGR carriers with a TLR. Features revealed include reduced cone densities, increased cone inner segment diameters, and increased rod outer segment reflectivity.

RETINA 0:1–11, 2017

Retinitis pigmentosa is a clinically heterogeneous group of progressive disorders characterized by night blindness and constriction of peripheral visual field in the early stages, leading to subsequent central visual loss, and is associated with over 100 different genes.[1–6] X-linked retinitis pigmentosa (XLRP) is often of earlier onset and more rapidly progressive than other forms, and accounts for between 10% and 20% of all cases, with 70% to 80% of these because of sequence variants in the retinitis pigmentosa GTPase regulator (*RPGR*) gene.[1,7–9] There are multiple *RPGR* isoforms arising from alternative splicing or posttranslational modification,[10] which are variably expressed in different tissues (lung, kidney, retina, brain, and testis), suggesting tissue-specific splicing with tissue-specific functions.[11] The 2 major isoforms are the constitutive *RPGR* exon 1 to 19 and *RPGR* ORF15, with the latter representing the most highly expressed in

photoreceptors.[12] Previous reports suggest that disease-causing variants are found in exons present in isoform *RPGR* ORF15, with only one in exons 15 to 19, supporting the importance of *RPGR* ORF15 in photoreceptors.[13–15] Although *RPGR* protein function is not completely characterized, it is believed to play a role in ciliary transport, with malfunction leading to early onset of visual symptoms usually in the first or second decade of life and progressing rapidly, with severe visual impairment by the fourth decade.[1,3,12,16]

Obligate XLRP carriers may either be asymptomatic or mildly affected, but are rarely as severely affected as men.[1,17–22] Observed deficits include visual field constriction[23] and loss of rod and cone responses on psychophysical testing[17,18] and electroretinography.[17,19,22] The most common observation in obligate XLRP carriers is a radial pattern of hyperreflectivity, frequently called a tapetal-like reflex (TLR). Unlike

a "true" tapetal reflex seen in the eyes of certain vertebrates,[24] which is a contiguous reflecting surface, the hyperreflectivity in XLRP carriers manifests as patchy radial streaks of golden-appearing retina.

A few studies have explored the appearance of the TLR and its cellular origin ex vivo and even fewer in vivo. Cideciyan and Jacobson[25] measured the size of hyperreflective particles by digitally magnifying film-based color fundus photographs, and deemed the hyperreflective particles to be consistent with the size of cone inner segments. A few years later, Berendschot et al[26] provided evidence that it was rather rod and cone photoreceptor outer segments that contribute to the TLR appearance in three XLRP carriers. More recently, Pyo Park et al[27] investigated XLRP carriers with a TLR (n = 5) using an adaptive optics scanning light ophthalmoscope (AOSLO) but without being able to resolve rods.

In this study, we have undertaken deep phenotyping of molecularly confirmed carriers of RPGR-associated RP. Color fundus photography, near-infrared (NIR) reflectance, fundus autofluorescence (FAF), spectral domain optical coherence tomography (SD-OCT), and confocal/nonconfocal AOSLO were used to explore the spatial correlation and composition of the fundus TLR. Here, we show that the TLR manifests as

1) increased reflectivity (or in other words, diminished local contrast) in the appearance of outer retinal bands in SD-OCT scans, and 2) bright reflecting rod photoreceptor outer segments, reduced cone densities, and enlarged cone inner segment diameters in AOSLO images of the photoreceptor mosaic.

Methods

Subjects

Nine molecularly confirmed RPGR carriers (28–62 years of age) and three noncarrier women (24–29 years of age) were enrolled. All carriers studied were from unrelated families. Seven consisted of the mothers of affected men, one was the sister of an affected man (MM_0010), and one was the maternal aunt of an affected man (MM_0039). The study adhered to the tenets of the Declaration of Helsinki and was approved by the Moorfields Eye Hospital Ethics Committee. Informed consent was obtained from all participants after explanation of the nature and potential consequences of the study before enrollment.

Pupils were dilated using one drop each of phenylephrine (2.5%) and tropicamide (1%) before retinal imaging. Axial length was measured using a Zeiss IOLMaster (Carl Zeiss Meditec, Jena, Germany) to correct the lateral scale of OCT and AOSLO images.

Retinal Spectral Domain Optical Coherence Tomography, Color Reflectance, Near-Infrared Reflectance, and Fundus Autofluorescence

All participants underwent SD-OCT using an Envisu system (Bioptigen, Morrisville, NC). Horizontal and vertical (where possible) rectangular (7 × 1 mm) volume scans (750 A-scans/B-scan, 10 B-scans/volume, each derived from an average of 15 frames) were acquired while asked to fixate on the center of a cross. The foveal center was estimated as the location where inner retinal thickness was minimal. At least 20 frames belonging to the foveal center were subsequently registered (to correct for eye motion) and averaged (to improve signal to noise ratio) using the ImageJ[28] plugin StackReg.[29]

Pixel intensities in the linear display (converted from the original logarithmic scale) were first measured for the outer retinal bands corresponding to the inner segment ellipsoid zone (EZ), outer segment interdigitation zone (IZ), and retinal pigment epithelium/Bruch membrane (RPE/BrM). A 5-pixel–wide longitudinal reflectivity profile was obtained (averaging the values across five

Reprint requests: Michel Michaelides, FRCOphth, UCL Institute of Ophthalmology, 11-43 Bath Street, London EC1V 9EL, United Kingdom; e-mail: michel.michaelides@ucl.ac.uk
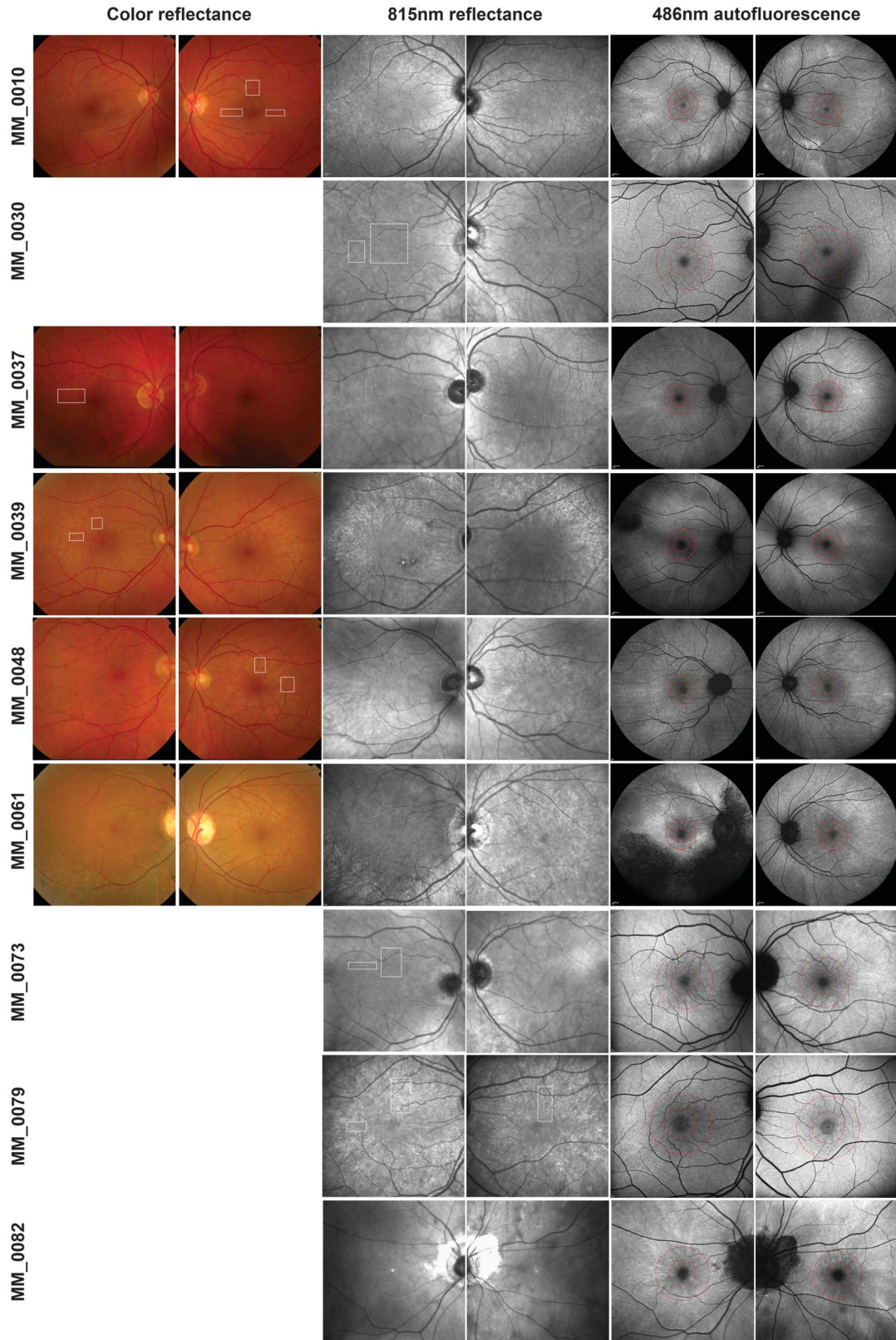
Fig. 1. Multimodal imaging in carriers of *RPGR*-associated RP. Color fundus photographs (where available), NIR reflectance, and FAF of all our *RPGR*-associated RP carriers. White rectangles indicate areas that were imaged with AOSLO on a cellular scale. The photoreceptor mosaic could not be resolved for MM_0061 and MM_0082. Concentric rings on FAF are centered on the fovea and correspond to 1 mm (inner) and 2 mm (outer) away from it to aid comparison across modalities (including OCT analysis).

Table 1. Clinical Characteristics and Genetic Results of *RPGR*-Associated RP Carriers (n = 9)

Carrier ID	Age	BCVA (OD, OS)	Moorfields Eye Hospital Pedigree	Exon	Mutation	Protein Change
MM_0010	28	6/5, 6/5	13724	Exon 8/Intron 8	c.836_934+1276del	Splicing
MM_0030	49	6/5, 6/6	20372	Exon 10	c.1243_1244delAG	p.Arg415Glyfs*37
MM_0037	43	6/48, 6/6	66	ORF15	c.2624_2643del20	p.Glu875Glyfs*197
MM_0039	62	6/5,6/9	4549	ORF15	c.2650 G>T	p.Glu884*
MM_0048	55	6/9, 6/9	180	ORF15	c.2045_2046dupGT	p.Arg683Valfs*15
MM_0061	62	6/12,6/9	18426	ORF15	c.2236_2237delGA	p.Glu746Argfs*23
MM_0073	34	6/6, 6/6	20844	ORF15	c.2405_2406delAG	p.Glu802Glyfs*32
MM_0079	52	6/5, 6/6	3878	ORF15	c.2907_2910delAGGA	p.Gly970Lysfs*118
MM_0082	47	6/6, 6/5	5201	ORF15	c.2238delA	p.Glu747Argfs*68

Reference sequence NM_001034853.1.
BCVA, best-corrected visual acuity; ORF, open reading frame.

consecutive lateral positions) at the foveal center (0 mm), and at 1 mm and 2 mm temporally/nasally/superiorly and inferiorly to the foveal center.[30] These locations were chosen to represent regions (in carriers) with a TLR (2 mm) and without a TLR (0 mm) and the respective transition zones (1 mm) as shown in Figure 1 with the aid of red concentric rings. Normalized local contrast was then calculated using a previously defined formula.[31] Comparison of these contrast values per eccentricity and retinal layer was performed by means of box plots (depicting the interquartile range, median, and whiskers extending out to 1.5 × interquartile range). Statistical analyses were conducted using Origin (OriginLab, Northampton, MA).

Subjects also underwent fundus color photography (macula centered, 50° field of view) using a mydriatic retinal camera (Topcon Ltd, Newbury, United Kingdom) and NIR (815 nm) reflectance fundus imaging (30° field of view) followed by blue (486 nm) FAF imaging (55 or 30° field of view) using the Heidelberg SPECTRALIS (Heidelberg Engineering, Heidelberg, Germany). Each FAF image was created from a registered average of at least 12 raw frames by means of the automatic real-time feature.

Photoreceptor Mosaic Imaging

At least one eye from each subject was imaged using a custom-built AOSLO that captured confocal images (focused on the outer segments of the photoreceptor layer) as previously described.[32] Briefly, the imaging light source was a 790-nm super luminescent diode (Superlum, Carrigtwohill, County Cork, Ireland), whereas wavefront sensing was performed using an 850-nm super luminescent diode (also from Superlum). Monochromatic wavefront aberrations were corrected using a 97-actuator deformable mirror (ALPAO, Biviers, France) with

a 14-mm clear aperture. Image sequences consisting of 150 frames were recorded at different locations across the central fovea and parafovea using a fixation target. The raw frames from these sequences were first desinusoided and then registered[33] before being manually tiled into a single montage (Adobe Photoshop CS6; Adobe Systems, Inc, San Jose, CA). Simultaneous confocal and nonconfocal split-detection AOSLO images[34] were obtained in absolute spatial and temporal registration during the follow-up of one carrier (MM_0048).

Tapetal-like reflex areas were identified in macroscopic modalities and guided the (microscopic) photoreceptor mosaic AOSLO imaging session to obtain TLR locations (white rectangles, Figure 1) for further cellular analysis. Two paired regions, one within a TLR area and another outside a TLR but adjacent to one (≤50 μm), were selected from seven *RPGR* carriers after acquisition. Matched eccentricities were used for analysis in the three noncarrier controls. All cone photoreceptors in the cropped regions (100 × 100 μm) were manually identified—their number was divided by that area to derive an estimate of the cone density for each image.

Serial photoreceptor mosaic images were obtained in a subset of carriers (MM_0037, MM_0039, and MM_0048) to longitudinally assess the TLR appearance on a cellular scale. Finally, with the aid of the nonconfocal split-detection AOSLO modality, cone (both outer and inner segments) and rod (outer segments) photoreceptors were identified in a TLR area (MM_0048) and their reflectivity values were measured. Pixel intensities from the center of all identified photoreceptors were plotted for direct comparison between cones and rods and between a carrier and an unaffected individual. If rod outer segments did not waveguide light back to the detector and thereby appeared dark
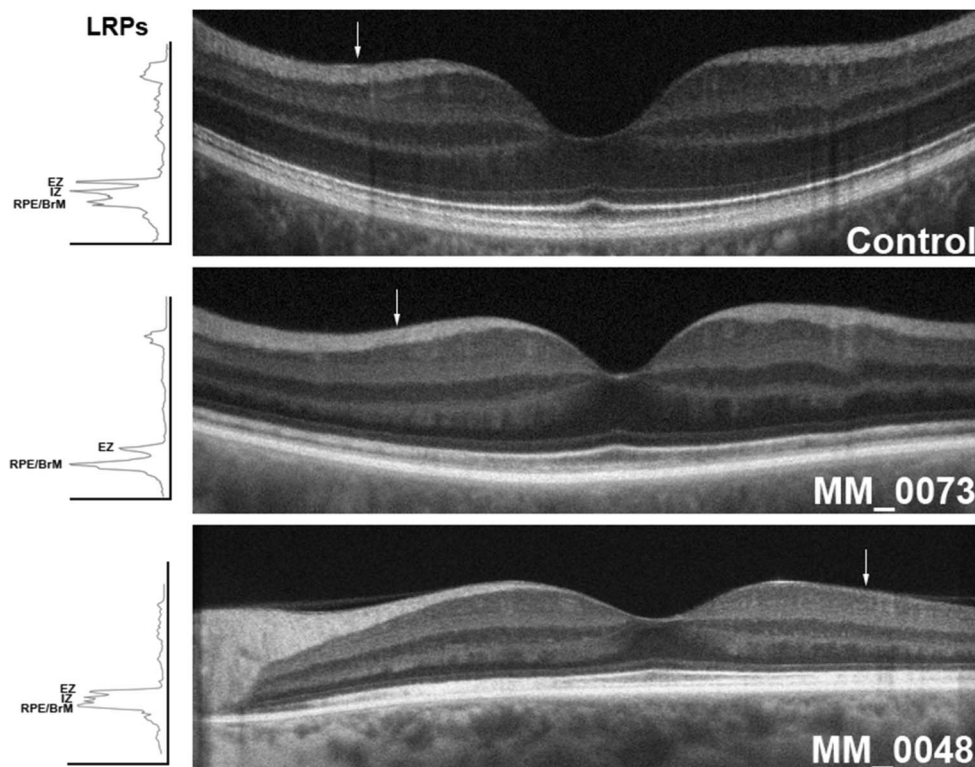
Fig. 2. Outer retinal SD-OCT local contrast measured in carriers with a TLR. Transfoveal SD-OCT scans from a non-carrier female control and two carriers with representative outer retinal layers exhibiting a TLR. White arrow on each image corresponds to the location of the five-pixel–wide longitudinal reflectivity profile shown to the left of the scans. Every arrow is 2 mm away from the foveal center. MM_0073's longitudinal reflectivity profile revealed 2 instead of 3 (as in the control scan, above) hyperreflective peaks. MM_0048's longitudinal reflectivity profile revealed all 3 outer retina layers but with diminished local contrast compared with the control. EZ, ellipsoid zone; IZ, interdigitation zone; RPE/BrM, retinal pigment epithelium/Bruch membrane.

in confocal AOSLO, they were not included in the reflectivity analysis because their exact location and number could not be identified from the nonconfocal image (because of their much smaller diameter), in direct contrast to cone photoreceptors. This also precluded any rod counting analysis.

Results

Carrier demographics, best-corrected visual acuity, and genotypes are summarized in Table 1. Ophthalmic appearances are shown in Figure 1. Carriers MM_0061 and MM_0082 were excluded from analysis due to poor scans/image quality and the inability to resolve photoreceptor mosaics in sufficient quality.

Color Fundus, Near-Infrared Reflectance, and Fundus Autofluorescence Retinal Imaging

Apart from color fundus images that were obtained in five of nine carriers, all other modalities were obtained in all *RPGR* carriers (Figure 1). In all carriers, a TLR was observed in color fundus (where available) and NIR reflectance, albeit to a varying intensity and extent, both between eyes of the same carrier and across carriers (intrafamilial variability and ocular asymmetry). Fundus autofluorescence imaging in our carrier cohort revealed radial patterns of increased autofluorescence signal in all images. These patterns did not always colocalize with the TLR areas observed in other modalities, but direct comparison could not be performed universally because of the different fields of view across modalities. None of the noncarrier controls showed a TLR in any modality. MM_0061 was severely affected, presenting with asymmetrical peripheral pigmentary changes, RPE atrophy, and vascular attenuation.

Outer Retinal Hyperreflective Bands on Spectral Domain Optical Coherence Tomography

Fundus TLR was associated with changes in appearance of the outer retinal layers (EZ and IZ) on SD-OCT (Figure 2). This is quantitatively analyzed and presented in Figure 3, which shows the contrast reduction in those layers while traversing from central (0 mm) non-TLR areas towards more peripheral (2 mm) TLR areas in all four directions (superior, inferior, temporal, and nasal). Asterisks denote statistically significant differences at the 0.05 level (paired t test). There was a significant reduction in the EZ local contrast between 0 mm (0.75 ± 0.1) and 2 mm (0.57 ± 0.1) inferiorly ($t(7) = 4.25$, $P = 0.0037$) and between 0 mm and 2 mm superiorly (0.59 ± 0.1) ($t(7) = 3.08$, $P = 0.017$). Similar significant contrast reductions were noted in the IZ layer between 0 mm (0.48 ± 0.09)
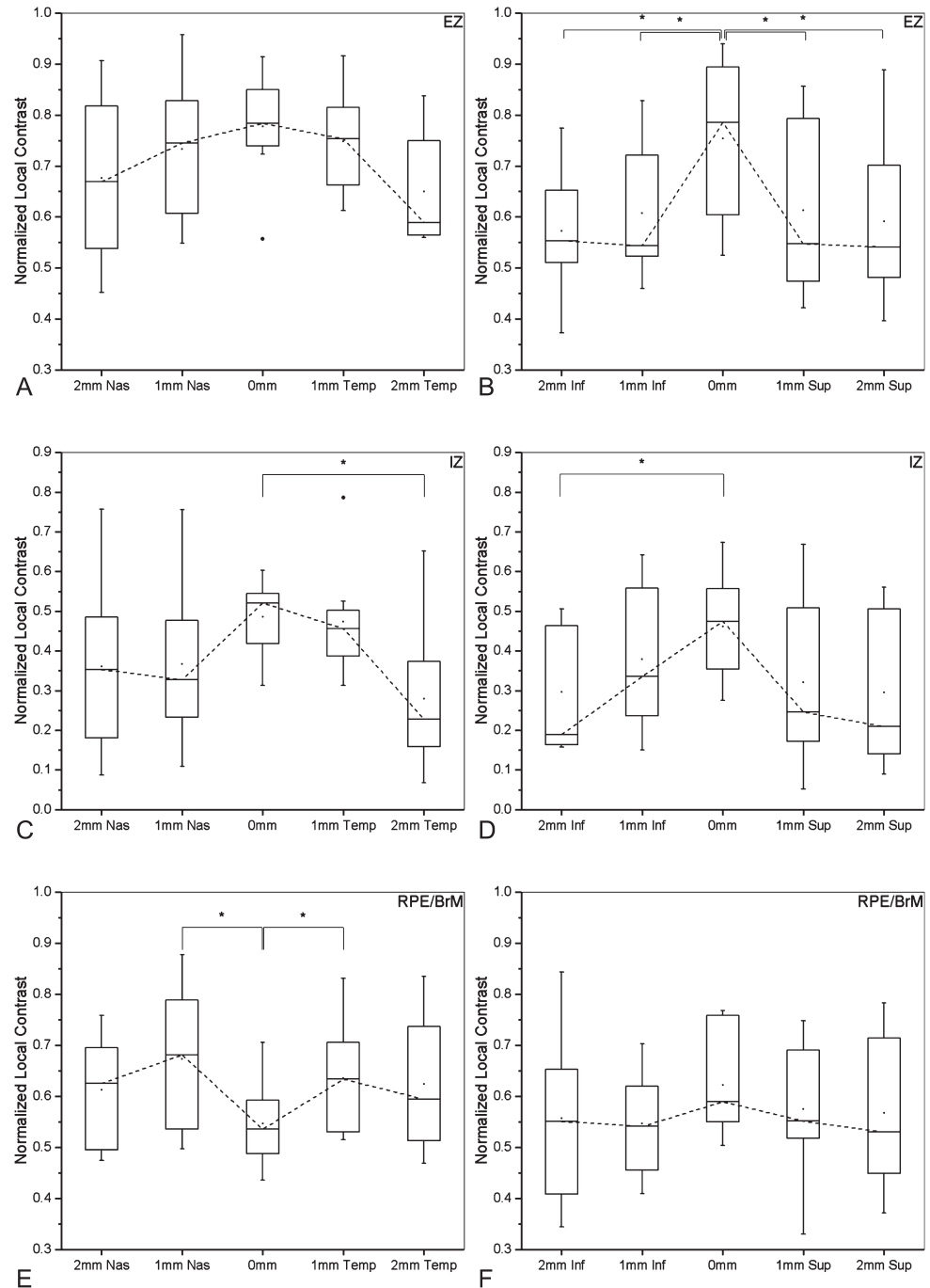
Fig. 3. Comparison of normalized local contrast across eccentricities for carriers exhibiting a TLR. Left column (**A**, **C** and **E**) plots are for horizontal and right column (**B**, **D** and **F**) are for vertical transfoveal SD-OCT line scans of carriers exhibiting a TLR with available SD-OCT scans. Box plots depict the interquartile range, median, and whiskers extend to 1.5 × interquartile range. Dashed lines join the median values. Filled squares indicate mean values and filled circles indicate outliers. Outer retina layers are designated as ellipsoid zone (EZ), interdigitation zone (IZ), and retinal pigment epithelium/ Bruch membrane (RPE/BrM), top to bottom rows. Normalized local contrast values at the foveal center (0 mm) were compared with those parafoveally at 1 mm and at 2 mm. Statistically significant differences are denoted with asterisks (paired *t* tests at the 0.05 level).

and 2 mm (0.27 ± 0.1) temporally (t(7) = 2.75, P = 0.028) and between 0 mm (0.46 ± 0.1) and 2 mm (0.31 ± 0.1) inferiorly (t(5) = 4.24, P = 0.008).

Qualitative and Quantitative Analysis of the Photoreceptor Mosaic

The photoreceptor mosaic could be resolved in the confocal AOSLO images from seven of nine carriers at

the regions of interest (eight eyes in total). The fundus TLR observed on color fundus and NIR reflectance images colocalized with areas of highly reflective rod photoreceptors in these seven carriers. Although the locations imaged by means of AOSLO (white rectangles, Figure 1) were chosen so as to represent TLR areas appearing in the macroscopic modalities, this could not be achieved in all cases (MM_0030 and MM_0073). Lack of color fundus images in these
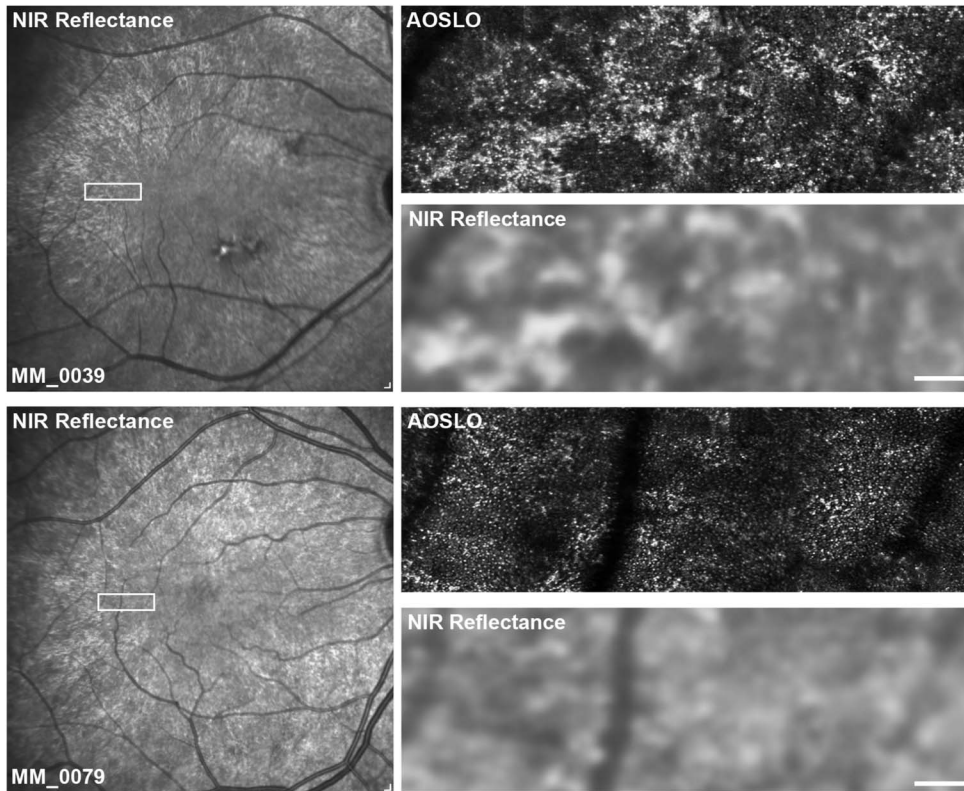
Fig. 4. Tapetal-like reflex appearance in carriers of RPGR-associated RP—colocalization of NIR reflectance and confocal AOSLO modalities. Shown are confocal AOSLO and matching NIR reflectance images from two carriers (MM_0039 and MM_0079). The rectangles on the NIR reflectance images indicate the areas enlarged on the right. The TLR patterns seen in NIR reflectance are clearly visible in the cellular arrangement, with rods of increased brightness in contrast to cones. Scale bars are 100 μm.

two carriers also hindered the confirmation of a TLR pattern macroscopically.

Cone photoreceptor density in the 14 regions of interest (2 each from 7 carriers) in TLR regions were, on average, 29.4% (range 12.9–47.8%) reduced compared with the immediately adjacent, non-TLR regions of interest (Figure 5). By contrast, six adjacent regions from the noncarrier controls (2 each from 3 controls) had an average difference of 1.7% (range 0.6–4.0%).

Reflectivity analysis of a TLR area in one of the carriers (MM_0048) approximately 2.2° away from the fovea revealed that 96% (24 of 25) of cone photoreceptor outer segments had a dim appearance of an average (±SD) intensity value of 103 (±48), whereas rod photoreceptor outer segments were on average (±SD) brighter (148 ± 80), with 39% of them (26 of 66) having intensities of at least 200 (see **Figure 1**, **Supplemental Digital Content 1**, http://links.lww.com/IAE/S774). Reflectivity values of cones (n = 83) and rods (n = 85) from an unaffected individual (MM_0136) were substantially lower (59 ± 20 and 21 ± 10, respectively). Carriers' cone photoreceptors have evidently enlarged inner segment diameters qualitatively illustrated in the nonconfocal image compared with the noncarrier control.

Longitudinal Observation of Tapetal-Like Reflex in the Photoreceptor Mosaic

Representative TLR appearances of the photoreceptor mosaic for the three carriers that were imaged 19 weeks apart (MM_0037 and MM_0039) and 42 weeks apart (MM_0048) are presented in **Supplemental Digital Content 2** (see **Figure 2**, http://links.lww.com/IAE/A775). The increased reflectivity of these TLR areas colocalized across time with no apparent brightness changes (qualitatively assessed).

Discussion

Fundus autofluorescence appearances in most of our carrier cohort showcased the radial patterns of increased AF in the rod-rich ring-shaped area around the fovea at the eccentricity of the optic disk, corroborating previous reports.[35,36] In some of our carriers, images are limited to a 30° field of view precluding confirmation of these patterns. Future relevant studies should aim for wider field of view (55°) FAF imaging.

Optical coherence tomography reflectivity analysis revealed reduced normalized contrast across outer retinal layers in TLR areas compared with non-TLR areas indicating higher reflectivity originating from the
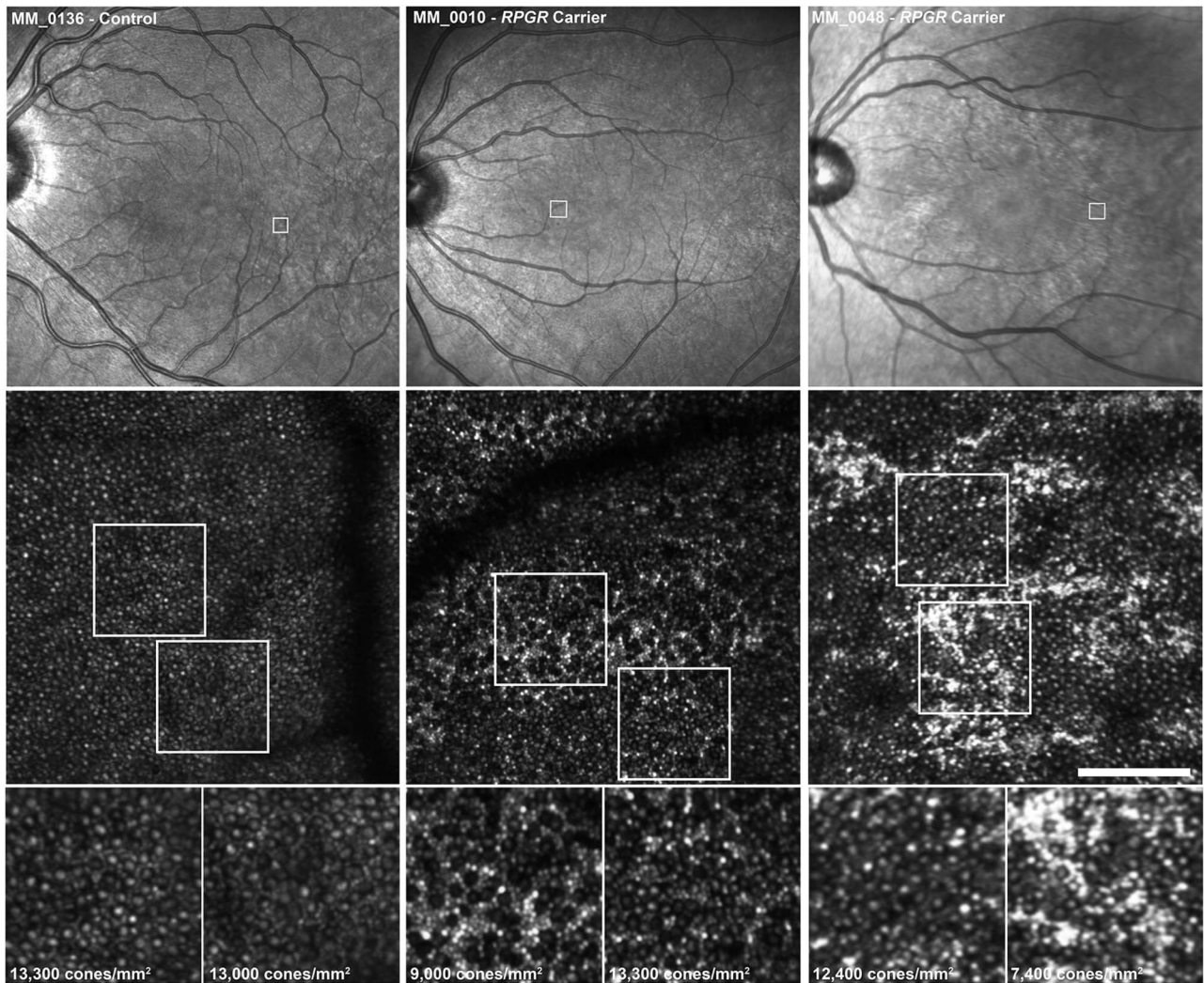
Fig. 5. Tapetal-like reflex areas are associated with localized cone loss compared with non-TLR areas in carriers of *RPGR*-associated RP. Shown is a region of temporal retina from a healthy control (MM_0136) and two *RPGR*-associated RP carriers with a highlighted region of interest (square, top row) in the nasal and temporal retina, respectively (MM_0010 and MM_0048) containing both TLR and non-TLR regions. These region of interests in the top row NIR reflectance images correspond to the location of the confocal AOSLO images below. The squares correspond to either regions of photoreceptor mosaic outside the TLR regions or to photoreceptor regions within the TLR. Scale bar is 100 μm. Adjacent regions in the noncarrier woman show virtually no difference in cone densities. Conversely, in *RPGR*-associated RP carriers the TLR regions are associated with decreased cone densities and increased rod outer segment brightness.

EZ and IZ photoreceptor interfaces. Because of the low transverse resolution of SD-OCT, it is not possible to distinguish the relative contribution of cones and rods populating these layers; hence, AOSLO imaging was the next step to achieve this goal.

Our study is the first to characterize the photoreceptor mosaic of TLR areas in *RPGR* carriers in vivo. Namely, the carriers' photoreceptor mosaic features are shown to comprise reduced cone densities within TLR areas compared with non-TLR areas, increased cone inner segment diameters compared with controls, and increased rod outer segment reflectivity compared with cone outer segments. Previous studies reported that the TLR likely originates from cone photorecep-

tors[25,27]; in our cohort, this was not the case, with only a very small percentage of cones appearing highly reflective (in direct contrast with rods). Overall, it seems that both rod and cone photoreceptors contribute toward the TLR, that is, are on average brighter than their noncarrier counterparts. Berendschot et al[26] were the first to report that the TLR originates at the outer segment of (both cone and rod) photoreceptors; our study provides evidence that more specifically it is almost exclusively rod photoreceptor outer segments (and not cones) which give the TLR appearance macroscopically (Figures 4 and 5). This conclusion is drawn from the evidence that high-resolution imaging offers: configuration of small

circular structures around larger cone-sized areas of reduced reflectivity (see **Figure 1**, **Supplemental Digital Content 1**, http://links.lww.com/IAE/S774). By definition, light from the RPE and inner segments is rejected by confocal AOSLO; hence, the rod outer segments alone are contributing to this increased reflectivity.

Whether the TLR appearance is the result of disruption of cones, rods, or both with/without other factors cannot be answered from this study. Functional testing in XLRP carriers has revealed that both cones and rods are equivalently affected[37,38]; however, because of the variability both between and within carriers (interocular), definitive conclusions cannot be drawn for all carriers.

Identifying the objects (here, rod outer segments) that appear brighter than their surroundings to give rise to the TLR appearance macroscopically does not necessarily answer a more complicated question of what is the cause of such appearance. Although our study was not designed to objectively establish the latter, we can suggest potential mechanisms of the origin of the TLR. The media surrounding rods (either the cones, or the organization of the RPE apical extensions, or both) may be disrupted in the form of an altered refractive index and this may in turn cause the TLR appearance partly because the rod signal is believed to depend on the refractive index difference between the interface of the rods and their surroundings. So, if the pair of adjacent media refractive indices closer matches one another (rather than differ), less light is waveguided and thus reflected (TLR).

Because the *RPGR* gene product has been shown to be ubiquitously expressed in tissue-specific splice forms,[10,12,39] at least two different hypotheses could hold true for the TLR mechanism. The first is that aberrant *RPGR* in the RPE alters the interaction between the apical appendages of the RPE cells and the rod outer segment tips, thus changing the refractive index and altering the observed signal. Second, *RPGR* expressed in the rod photoreceptors alters their shape and composition (because of trafficking defects) and thus, changes their interaction with the RPE and the optical signal they generate, as has been suggested in Oguchi disease.[40] However, multiple studies have sought to identify *RPGR* expression patterns; the ORF15 containing isoform is only found in photoreceptors.[10,39] This suggests that *RPGR* expressed in RPE is likely a different isoform than that expressed in photoreceptors and is potentially unaffected by the ORF15 sequence variants in most of our carriers' cohort. Further work from Beltran et al suggested both

cone and rod opsin mislocalization (in the same retinal patches) to the inner segments and outer nuclear layer in two canine models of *RPGR*-associated disease.[41] If such structural changes exist and to what extent they affect the appearance of the photoreceptor mosaic in *RPGR* carriers remains to be elucidated.

Our results corroborate ex vivo retinal histopathology studies in *RPGR* carriers (humans and animal models) showing reduction in photoreceptor numbers.[41–43] In addition, loss of the outer segment, nonuniform cone spacing, and both shorter and broader cone inner segments (similar rod changes, but to a lesser extent) have been documented throughout the retina, including the perifoveal region. To assess outer segment length in vivo, AO-OCT would prove a complementary imaging modality with better axial and lateral resolution compared with SD-OCT toward a more complete and precise characterization of outer retinal structure in *RPGR* carriers.

The increased reflectivity of the rod outer segments in confocal AOSLO images was broadly consistent across all seven carriers. An area that should be further explored in the future is microperimetry in TLR areas.[20,44] Previous studies suggest that there was a reduction in photopic and scotopic performance in TLR areas; however, stimuli positioning may have not been accurate enough to exclusively target small streaks of such golden strands. New, adaptive optics and high-fidelity eye-tracking schemes allow stimulus presentation with cellular precision[45] and have been demonstrated in other retinal conditions.[46] Application of these techniques in *RPGR* carriers expressing patterns of fundus TLR would be informative.

Our study has some limitations. First, we did not obtain color retinal photographs from four carriers to assess the full macroscopic TLR appearance across our cohort. Second, we did not control for the adaptation state (photopic versus scotopic vision) before each imaging modality[47] to compensate for potential fluctuations of the TLR appearance with varying retinal exposure to light. Nevertheless, we have (qualitatively) shown that three of our carriers showed no fluctuations in TLR intensities across visits. Third, our sample size was relatively limited (n = 7), albeit —to the best of our knowledge—it is the only study with in vivo cellular imaging down to rod resolution. Lastly, the lack of nonconfocal split-detection AOSLO imaging for all but one of the carriers precluded the expansion of our photoreceptor reflectivity analysis because of the challenges in reliably discriminating between cone and rod photoreceptors, as well as distinguishing neighboring bright rods as individual photoreceptors rather than potentially confusing them for cones, using the confocal modality alone.

Cideciyan and Jacobson[25] drew attention to the increased reflectivity in color fundus reflectance images taken in XLRP carriers, and this finding has been supported by other imaging studies. Structural and functional cellular mosaicism because of random X-chromosome inactivation has also been reported in other X-linked conditions such as cone dystrophy, blue cone monochromatism, X-linked retinoschisis, and choroideremia.[48–52] We extend these aforementioned observations in a cohort of molecularly confirmed carriers of XLRP harboring disease-causing sequence variants in *RPGR* and provide evidence that cone density is reduced in TLR areas compared with adjacent non-TLR ones and that increased rod outer segment reflectivity accounts for the observed TLR in these same areas. It remains to be determined whether baseline photoreceptor TLR and associated cellular changes observed on AOSLO are prognostic indicators of the magnitude and/or rate of progression a carrier may experience over time.

Key words: adaptive optics, carriers, heterozygotes, imaging, retinitis pigmentosa, tapetal-like reflex.

References

1. Bird AC. X-linked retinitis pigmentosa. Br J Ophthalmol 1975; 59:177–199.
2. Churchill JD, Bowne SJ, Sullivan LS, et al. Mutations in the X-linked retinitis pigmentosa genes *RPGR* and *RP*2 found in 8.5% of families with a provisional diagnosis of autosomal dominant retinitis pigmentosa. Invest Ophthalmol Vis Sci 2013;54:1411–1416.
3. Daiger SP, Sullivan LS, Bowne SJ. Genes and mutations causing retinitis pigmentosa. Clin Genet 2013;84:132–141.
4. Ebenezer ND, Michaelides M, Jenkins SA, et al. Identification of novel *RPGR* ORF15 mutations in X-linked progressive cone-rod dystrophy (XLCORD) families. Invest Ophthalmol Vis Sci 2005;46:1891–1898.
5. Fishman G, Farber M, Derlacki D. X-linked retinitis pigmentosa profile of clinical findings. Arch Ophthalmol 1988;106: 369–375.
6. Hartong DT, Berson EL, Dryja TP. Retinitis pigmentosa. Lancet 2006;368:1795–1809.
7. Berger W, Kloeckener-Gruissem B, Neidhardt J. The molecular basis of human retinal and vitreoretinal diseases. Prog Retin Eye Res 2010;29:335–375.
8. Shu X, Black GC, Rice JM, et al. *RPGR* mutation analysis and disease: an update. Hum Mutat 2007;28:322–328.
9. Tee JJL, Smith AJ, Hardcastle AJ, Michaelides M. *RPGR*-associated retinopathy: clinical features, molecular genetics, animal models and therapeutic options. Br J Ophthalmol 2016;100:1022–1027.
10. Yan D, Swain PK, Breuer D, et al. Biochemical characterization and subcellular localization of the mouse retinitis pigmentosa GTPase regulator (mRpgr). J Biol Chem 1998;273: 19656–19663.
11. Kirschner R, Rosenberg T, Schultz-Heienbrok R, et al. *RPGR* transcription studies in mouse and human tissues reveal a retina-specific isoform that is disrupted in a patient with X-linked retinitis pigmentosa. Hum Mol Genet 1999;8:1571–1578.
12. He S, Parapuram SK, Hurd TW, et al. Retinitis pigmentosa GTPase regulator (*RPGR*) protein isoforms in mammalian retina: insights into X-linked retinitis pigmentosa and associated ciliopathies. Vis Res 2008;48:366–376.
13. Ayyagari R, Demirci F, Liu J, et al. X-linked recessive atrophic macular degeneration from *RPGR* mutation. Genomics 2002; 80:166–171.
14. Vervoort R, Lennon A, Bird AC, et al. Mutational hot spot within a new *RPGR* exon in X-linked retinitis pigmentosa. Nat Genet 2000;25:462–466.
15. Vervoort R, Wright AF. Mutations of *RPGR* in X-linked retinitis pigmentosa (RP3). Hum Mutat 2002;19:486–500.
16. Wright AF, Shu X. Focus on molecules: *RPGR*. Exp Eye Res 2007;85:1–2.
17. Berson EL, Rosen JB, Simonoff EA. Electroretinographic testing as an aid in detection of carriers of X-chromosome-linked retinitis pigmentosa. Am J Ophthalmol 1979;87:460–468.
18. Ernst W, Clover G, Faulkner DJ. X-linked retinitis pigmentosa: reduced rod flicker sensitivity in heterozygous females. Invest Ophthalmol Vis Sci 1981;20:812–816.
19. Fishman G, Weinberg A, McMahon T. X-linked recessive retinitis pigmentosa: clinical characteristics of carriers. Arch Ophthalmol 1986;104:1329–1335.
20. Genead MA, Fishman GA, Lindeman M, et al. Structural and functional characteristics in carriers of X-linked retinitis pigmentosa with a tapetal-like reflex. Retina 2010;30:1726–1733.
21. Kousal B, Skalicka P, Valesova L, et al. Severe retinal degeneration in women with a c.2543del mutation in ORF15 of the *RPGR* gene. Mol Vis 2014;20:1307–1317.
22. Vajaranant TS, Seiple W, Szlyk JP, Fishman GA. Detection using the multifocal electroretinogram of mosaic retinal dysfunction in carriers of X-linked retinitis pigmentosa. Ophthalmology 2002;109:560–568.
23. Grover S, Fishman GA, Anderson RJ, Lindeman M. A longitudinal study of visual function in carriers of X-linked recessive retinitis pigmentosa. Ophthalmology 2000;107:386–396.
24. Nicol J. Vertebrate photoreceptor optics. In: Tapeta Lucida of Vertebrates. Berlin, Germany: Springer-Verlag; 1981: 401–431.
25. Cideciyan AV, Jacobson SG. Image analysis of the tapetal-like reflex in carriers of X-linked retinitis pigmentosa. Invest Ophthalmol Vis Sci 1994;35:3812–3824.
26. Berendschot TT, DeLint PJ, van Norren D. Origin of tapetal-like reflexes in carriers of X-linked retinitis pigmentosa. Invest Ophthalmol Vis Sci 1996;37:2716–2723.
27. Pyo Park S, Hwan Hong I, Tsang SH, Chang S. Cellular imaging demonstrates genetic mosaicism in heterozygous carriers of an X-linked ciliopathy gene. Eur J Hum Genet 2013;21: 1240–1248.
28. Abramoff M, Magalhaes P, Ram S. Image processing with ImageJ. Biophot Int 2004;11:36–43.

29. Thevenaz P, Ruttimann UE, Unser M. A pyramid approach to subpixel registration based on intensity. IEEE Trans Image Process 1998;7:27–41.

30. Huang Y, Cideciyan AV, Papastergiou GI, et al. Relation of optical coherence tomography to microanatomy in normal and *rd* chickens. Invest Ophthalmol Vis Sci 1998;39:2405–2416.

31. Tanna H, Dubis AM, Ayub N, et al. Retinal imaging using commercial broadband optical coherence tomography. Br J Ophthalmol 2010;94:372–376.

32. Dubra A, Sulai Y. Reflective afocal broadband adaptive optics scanning ophthalmoscope. Biomed Opt Express 2011;2:1757–1768.

33. Dubra A, Harvey Z. Registration of 2D images from fast scanning ophthalmic instruments. In: Biomedical Image Registration. Berlin, Heidelberg: Springer; 2010:60–71.

34. Scoles D, Sulai YN, Langlo CS, et al. In vivo imaging of human cone photoreceptor inner segments. Invest Ophthalmol Vis Sci 2014;55:4244–4251.

35. Ogino K, Oishi M, Oishi A, et al. Radial fundus autofluorescence in the periphery in patients with X-linked retinitis pigmentosa. Clin Ophthalmol 2015;9:1467–1474.

36. Wegscheider E, Preising MN, Lorenz B. Fundus autofluorescence in carriers of X-linked recessive retinitis pigmentosa associated with mutations in *RPGR*, and correlation with electrophysiological and psychophysical data. Graefes Arch Clin Exp Ophthalmol 2004;242:501–511.

37. Jacobson SG, Yagasaki K, Feuer WJ, Román AJ. Interocular asymmetry of visual function in heterozygotes of X-linked retinitis pigmentosa. Exp Eye Res 1989;48:679–691.

38. Peachey NS, Fishman GA, Derlacki DJ, Alexander KR. Rod and cone dysfunction in carriers of X-linked retinitis pigmentosa. Ophthalmology 1988;95:677–685.

39. Trifunovic D, Karali M, Camposampiero D, et al. A high-resolution RNA expression atlas of retinitis pigmentosa genes in human and mouse retinas. Invest Ophthalmol Vis Sci 2008;49:2330–2336.

40. Godara P, Cooper RF, Sergouniotis PI, et al. Assessing retinal structure in complete congenital stationary night blindness and Oguchi disease. Am J Ophthalmol 2012;154:987–1001.

41. Beltran WA, Acland GM, Aguirre GD. Age-dependent disease expression determines remodeling of the retinal mosaic in carriers of *RPGR* exon ORF15 mutations. Invest Ophthalmol Vis Sci 2009;50:3985–3995.

42. Aguirre GD, Yashar BM, John SK, et al. Retinal histopathology of an *XLRP* carrier with a mutation in the *RPGR* exon ORF15. Exp Eye Res 2002;75:431–443.

43. Adamian M, Pawlyk BS, Hong DH, Berson EL. Rod and cone opsin mislocalization in an autopsy eye from a carrier of X-linked retinitis pigmentosa with a gly436Asp mutation in the RPGR gene. Am J Ophthalmol 2006;142:515–518.

44. Acton JH, Greenberg JP, Greenstein VC, et al. Evaluation of multimodal imaging in carriers of X-linked retinitis pigmentosa. Exp Eye Res 2013;113:41–48.

45. Tuten WS, Tiruveedhula P, Roorda A. Adaptive optics scanning laser ophthalmoscope-based microperimetry. Optom Vis Sci 2012;89:563–574.

46. Wang Q, Tuten WS, Lujan BJ, et al. Adaptive optics microperimetry and OCT images show preserved function and recovery of cone visibility in macular telangiectasia type 2 retinal lesions. Invest Ophthalmol Vis Sci 2015;56:778–786.

47. Bregnhøj J, Al-Hamdani S, Sander B, et al. Reappearance of the tapetal-like reflex after prolonged dark adaptation in a female carrier of *RPGR* ORF15 X-linked retinitis pigmentosa. Mol Vis 2014;20:852–863.

48. Heckenlively J, Weleber R. X-linked recessive cone dystrophy with tapetal-like sheen: a newly recognized entity with Mizuo-Nakamura phenomenon. Arch Ophthalmol 1986;104:1322–1328.

49. de Jong P, Zrenner E, van Meel G, et al. Mizuo phenomenon in X-linked retinoschisis: pathogenesis of the Mizuo phenomenon. Arch Ophthalmol 1991;109:1104–1108.

50. Carroll J, Rossi EA, Porter J, et al. Deletion of the X-linked opsin gene array locus control region (LCR) results in disruption of the cone mosaic. Vis Res 2010;50:1989–1999.

51. Rossi EA, Achtman RL, Guidon A, et al. Visual function and cortical organization in carriers of blue cone monochromacy. PLoS One 2013;8:1–17.

52. Vajaranant TS, Fishman GA, Szlyk JP, et al. Detection of mosaic retinal dysfunction in choroideremia carriers electroretinographic and psychophysical testing. Ophthalmology 2008;115:723–729.